High Speed Visualization of Droplets Impacting with a Dry Surface at High Weber Numbers

Chapter · January 2018

DOI: 10.1007/978-3-319-64519-3_46

2 authors, including:

David Burzynski
Coldsense Technologies
9 PUBLICATIONS **203** CITATIONS

SEE PROFILE

High Speed Visualization of Droplets Impacting with a Dry Surface at High Weber Numbers

David A. Burzynski and Stephan E. Bansmer

Abstract The focus of this article is to describe the evolution of the spreading diameter and secondary droplets generated by splashing. High-speed visualization was used to study the time evolution of water droplets impacts with dry surfaces at Weber numbers between 3,500 and 10,000. Different prediction models of the maximal spreading diameter have been compared with each other and with the experimental data. A similarity between the spreading rates was observed in the last stage of the impact at high Weber numbers. The time evolution of the secondary droplets and the formation of the crown was observed and analyzed at the different Weber numbers.

1 Introduction

When a droplet impacts with solid surfaces at high velocities, a part of the droplet's mass sticks on the surface, forming a thin film. The other part of the mass atomizes into small secondary droplets. This phenomenon is called splashing. It is an important fundamental process for a wide range of technical applications, such as coating, vehicle soiling, or aircraft icing [1]. For all these applications, it is crucial to describe both the mass of the droplet that sticks and the total mass of the secondary droplets. During the initial impact phase, the thin film formed by the mass that has stuck spreads radially over the surface. This amount of spreading is described by the rim diameter, commonly called the spreading diameter [9]. Consequently, this film generates an ejecta sheet that develops into secondary droplets [11]. The film can also separate itself from the surface, creating a crown. This crown atomizes into more secondary droplets during the spreading process due to capillary instabilities [11]. A review of the recent theoretical, numerical, and experimental investigations of droplets impacting with a solid surface can be found in [5].

Many parameters affect the splashing on dry solid surfaces. However, the inertial forces dominate the behavior of water droplets that impact with a dry surface at high velocity. The impact dynamics are characterized using the Weber and Reynolds numbers [5]. The Weber number is the ratio between the inertial and capillary forces, and the Reynolds number represents the ratio between inertial and viscous forces. The characteristic numbers are defined as

$$We = \frac{\rho u_{imp}^2 d_d}{\sigma} \qquad \text{and} \qquad Re = \frac{u_{imp} d_d}{\nu}, \tag{1}$$

David A. Burzynski · Stephan E. Bansmer
Technische Universität Braunschweig, Institute of Fluid Mechanics, Hermann-Blenk-Str. 37, 38108 Braunschweig, e-mail: d.burzynski@tu-bs.de

where ρ is the liquid density, d_d is the droplet diameter, u_{imp} is the impact velocity, σ is the liquid surface tension, and ν is the kinematic viscosity of the liquid.

A host of investigations have been carried out over the last decades, although until now they have only studied the splashing at relatively low Weber numbers $We < 2,500$. This is relevant for many applications, but for vehicle soiling or aircraft icing, where the impact velocities and the droplet diameters are high, the related Weber number is higher than 3,000 [4], [12]. One of the few experimental investigations for $We \approx 22,000$ was performed by Mehdizadeh et al. [6], in which the fingering phenomenon was observed. Later, Mehdizadeh et al. [7] observed that the maximum spreading diameter increased with the temperature. More recently, another experimental investigation was performed by Fassmann et al. [3]. In this study, the secondary droplets were analyzed using a shadowgraph and statistical techniques for $We = 3,500$, $We = 5,000$, and $We = 10,000$. However, the investigations were performed using only double-frame images, and a complete time evolution of splashing as well as the spreading diameter at those Weber numbers has not been performed yet.

The dimensionless spreading diameter $\beta = d_r/d_d$ describes the radial expansion of the thin fluid film generated by the amount of droplet mass stuck on the surface. Different models have been proposed to predict β as a function of the parameters presented in Eq. 1. A detailed description of the time evolution was introduced by Rioboo et al. [8], showing that the spreading is classified in four different phases (kinematic, spreading, relaxation, and wetting phase). Typically, the time is made dimensionless using the impact velocity and the droplet diameter to obtain similarity. The dimensionless time is defined as $\tau = t u_{imp}/d_d$.

In addition to this splashing classification, Sheller et al. [10] suggested a model for β_{max} proportional to the Reynolds and Weber numbers for a wide range of liquids. Their model predicts the spreading diameter for experiments at low Weber number. A model based only on the Weber numbers was introduced later by Clanet et al. [2]. They studied spreading on super-hydrophobic surfaces. This simple model was developed using mass conservation arguments. Another interesting model has been recently introduced by Roisman [9]. He developed a semi-empirical expression using the thickness of the viscous boundary layer. Similar to Sheller et al. [10], this model predicts the maximal spreading diameter directly from the Weber and Reynolds numbers, although from a theoretical point of view instead of only using empirical data. Table 1 summarizes these three models.

Table 1: Models of the maximal spreading diameter β_{max} in terms of We and Re

Model	Spreading diameter
Scheller	$\beta_{max} \sim 0.61 Re^{1/5} (WeRe^{-2/5})^{1/6}$
Clanet	$\beta_{max} \sim We^{1/4}$
Roisman	$\beta_{max} \sim 0.87 Re^{1/5} - 0.4 Re^{2/5} We^{-1/2}$

Although different studies have been carried out in this area, there is no information about the time evolution of splashing and the spreading diameter at high Weber numbers. The goal of the present work is to close this gap of information, analyzing the splashing in detail for three different regimes: $We = 3,500$, $We = 5,000$, and $We = 10,000$. The Weber numbers were chosen according to Faßmann et al. [3]. The outcome of this work would help to develop new theoretical models and validate numerical simulations. Thus, the maximal spreading diameter and the secondary droplets were studied to contribute to the understanding of splashing at high Weber numbers. The development of the maximal spreading diameter β_{max} was determined experimentally as shown in 3(c). The results were compared with the different models from Table 1. Additionally, the time evolution of the crown and secondary droplets was observed from two different camera positions. These observations allow a qualitative comparison of the amount of generated droplets.

2 Experimental Methods

High Weber numbers were obtained by increasing the impact velocity using a flywheel, see Figure 1. The substrate was mounted on the motor-driven flywheel, and the droplets were generated at $y = 0.8$ m from the substrate position. Since this position was not changed, the angular velocity of the flywheel was increased for higher Weber number.

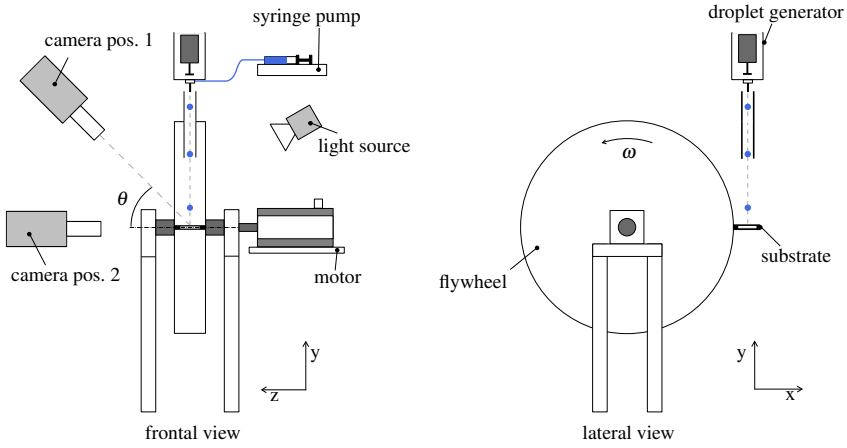

Fig. 1: Experimental set-up: The motor-driven flywheel rotates at constant angular velocity ω. A droplet is formed and falls due to gravity until it impacts with the substrate mounted on the flywheel. The splashing is recorded with one high-speed camera at two different positions ($\theta = 40°$ and $\theta = 0°$). The light source is positioned in order to reflect the light off the secondary droplets and rim.

In this setup, the flywheel rotated at the desired angular velocity ω, while a droplet was formed by gravity in the droplet generator. Then, the droplet was released and it fell under the influence of gravity; after some milliseconds the droplet

impacted with the substrate. Additionally, the droplets were protected by an acrylic glass shielding tube from the turbulent air flow created by the flywheel. Using this method, it was possible to reproduce the impact of distilled water droplets on a glass substrate ($R_a = 11$ nm and $R_z = 608$ nm) at ambient conditions ($T = 17.2 \pm 0.4$°C and $p = 1001.4 \pm 0.8$ hPa) several times.

The droplet generator consists of a syringe pump, a needle, a polyurethane hose, and a cage with a solenoid. The syringe pump KDS200 from KD Scientific was used to regulate the volume rate. The syringe was connected to the needle under the cage through the polyurethane hose. After a specific amount of water was pumped into the needle, the droplet was formed and hung until the cage was hit by the solenoid. Subsequently, the droplet separated from the needle and fell under the influence of gravity.

A Standford DG535 delay generator was used to synchronize the droplet generator and cameras to the flywheel. This was done in four steps. First, the trigger signal was generated by a light barrier mounted on the flywheel and sent to the delay generator. Second, a signal was sent from the delay generator to the solenoid to release the droplet. Third, another signal was sent some milliseconds later to the camera to record the events. Finally, the last signal was sent to the syringe pump to form a new droplet.

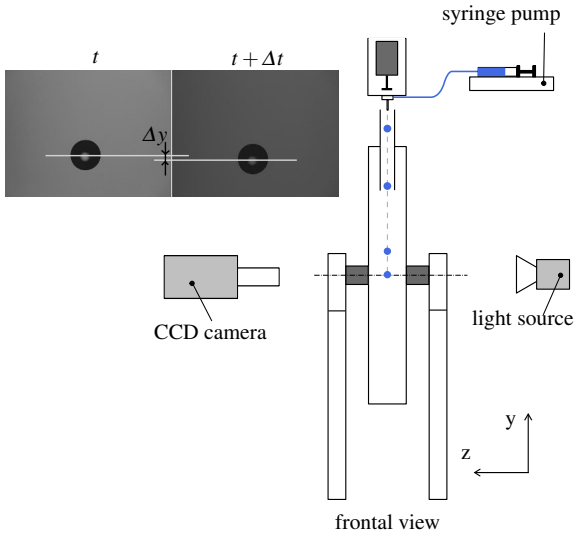

Fig. 2 Shadowgraph set-up: a droplet is formed and released by the generator. The droplet is released and falls under the influence of gravity. Just before it impacts with the substrate, the diameter and velocity are measured by means of shadowgraphy using a CCD-camera and Nd:YAG laser. Images show the double-frame pictures obtained and how the velocity is basically calculated $u_d = \Delta y / \Delta t$.

The shadowgraph technique was used first to determine the diameter, the position, and the velocity of the falling droplets as shown in Figure 2. The angular velocity of the flywheel was adjusted on the basis of this information in order to achieve the desired Weber number. With the objective to obtain well-detailed information about the droplet before the impact, a double-frame CCD camera with a resolution of 4,008 x 2,672 pixel was used together with a Nd:YAG laser with diffuser optics from LaVision GmbH. Thereafter, the raw images were processed using the software DaVis ParticleMaster, also from LaVision. As a result of these measurements, the substrate velocity was set to $u_s = 6.382 \pm 0.014$ m/s, $u_s = 8.259 \pm 0.007$ m/s, and

$u_s = 13.018 \pm 0.004$ m/s to achieve the Weber numbers $We = 3,500$, $We = 5,000$, and $We = 10,000$, respectively.

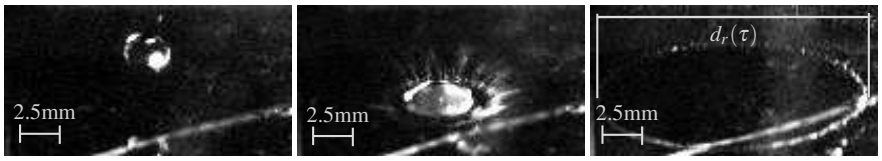

(a) $\tau < 0$ (b) $\tau > 0$ (c) $\tau \gg 0$

Fig. 3: Determination of the spreading diameter β: Perspective view from position 1 of a droplet impacting at We=5,000. Images were recorded using the high-speed camera at 32,000fps. (a) the droplet before the impact, (b) the formation of the secondary droplets and jets, and (c) the estimation of the rim diameter d_r.

Finally, the main observations were made using an HPV-2 high-speed camera from Shimadzu from two different positions as shown in Figure 1. The field of view was illuminated by a conventional halogen lamp. The camera at position 1 ($\theta = 40°$) was used to observe the spreading diameter, the rate, and the evolution of the rim and fingerings. The spreading diameter d_r was then estimated as shown in Figure 3. The secondary droplets and the formed thin crown were observed using the camera at position 2 ($\theta = 0°$). The recording rate of the camera was varied from 32,000 to 63,000fps for different Weber numbers. All cameras were calibrated using a target plate ParticleMaster from LaVision. Moreover, the perspective error was reduced using predefined and measured marks on the substrate.

3 Results

Figure 4 shows the spreading diameter β as a function of the dimensionless time τ for low and high Weber numbers. The results obtained by Rioboo et al. [8] at low Weber numbers are plotted together with the results of this study. This figure shows that not only the maximal spreading diameter β_{max} increases along with an increasing Weber number, but also the time to reach this value. While at lower Weber numbers β_{max} is found at $\tau \approx 1$, at high Weber numbers the β_{max} is found after $\tau > 4$. This behavior agrees with all the models presented in Sec. 1, which predict an increase in the maximal spreading diameter along with the increase of Weber numbers.

A detailed analysis of the data obtained at high Weber numbers, as shown in Figure 5, shows that the rate of the spreading diameter increase is almost the same for all cases ($We > 3,500$). This behavior has a logarithmic character until $\tau \approx 2$. This similarity is independent of the Weber number and was not expected because it did not appear in the experiments performed by Rioboo et al. [8]. This shows that the behavior for low Weber number cannot be easily related to higher values. However, at the final stage ($\tau \approx 5$), the spreading diameter differs for each Weber number until it reaches β_{max}. These observations agree with the theoretical models, where multiple analysis yielded that $\beta_{max} \sim We$.

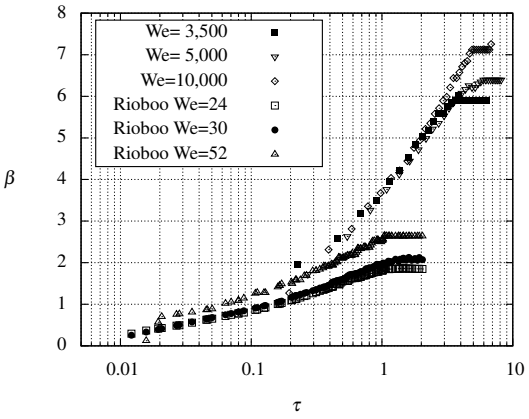

Fig. 4 Spreading diameter β of a mono-disperse water droplet impacting with a dry glass surface as a function of the dimensionless time τ for different Weber numbers. Experimental results obtained at $We = 3,500$, $We = 5,000$, and $We = 10,000$ compared with the experiments of Rioboo et al. [8] for low Weber numbers.

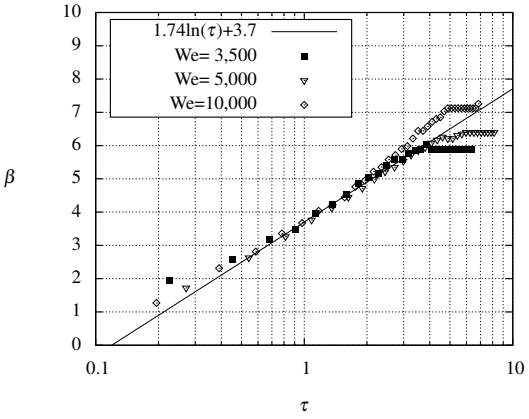

Fig. 5 Spreading diameter β of a mono-disperse water droplet impacting with a dry glass surface as a function of the dimensionless time τ for different Weber numbers. The spreading diameter develops similarly to the logarithmic fitting function and independently of the Weber number for $0.5 < \tau < 3$.

Figure 6 shows the spreading rate $\dot{\beta} = \partial\beta/\partial\tau$ over the dimensionless time τ. The measurements show that, starting from $\tau \approx 0.5$, the spreading rate is similar for all Weber numbers. This rate is approximated by a rational function (Eq. 2). It is possible to calculate the deceleration $\ddot{\beta} = \partial\dot{\beta}/\partial\tau$ of the spreading diameter. The deceleration in Figure 7 obtained using forward difference quotients demonstrates the same character that the measurements obtained at $We = 5,000$. Note that deceleration is caused by the surface tension and viscous dissipation. This information would contribute to future theoretical analysis, where the radial spreading force is taken into account.

$$\frac{\partial\beta}{\partial\tau} \approx \frac{2.16}{(0.18+0.96\tau)^{1.27}} \tag{2}$$

As discussed in Section 1, a host of models have been introduced over the last decades to describe the maximal spreading diameter as a function of different dimensionless parameters. The maximal spreading diameter predicted by these mod-

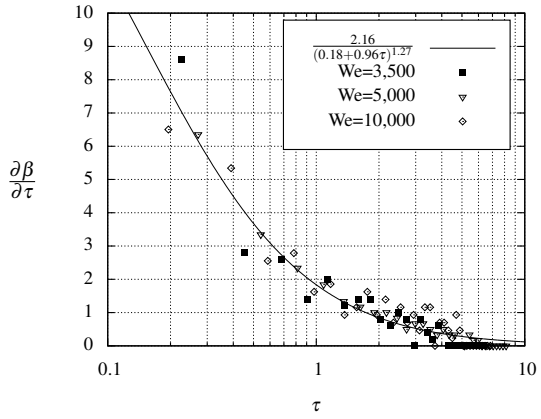

Fig. 6 Spreading rate $\dot{\beta}$ of a mono-disperse water droplet impacting with a dry glass surface as a function of the dimensionless time τ for different high Weber numbers. The independence of the spreading rate on the Weber numbers is described by a rational function (Eq. 2).

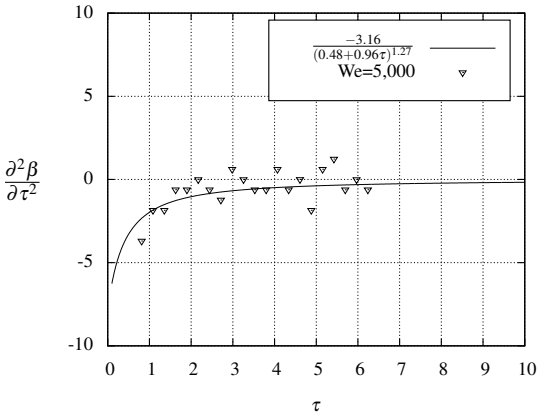

Fig. 7 Spreading acceleration $\ddot{\beta}$ of a mono-disperse water droplet impacting with a dry glass surface as a function of the dimensionless time τ for We=5,000. The curve represents the time derivative of Eq. 2.

els is illustrated in Figure 8 for high Weber numbers. Some discrepancies between the models presented by Sheller and Clanet and the measurements are observed. The biggest difference is observed at $We = 10,000$, where Sheller and Clanet models overestimate the measurements by 67% and 40% respectively. However, the model presented by Roisman predicts the maximal spreading diameter accurately. According to these results, the correct way to characterize β_{max} at high Weber number is to consider the viscous boundary layers during the impact, as shown in [9]. Moreover, this experimental validation opens the way for new theoretical studies that could predict the number of secondary droplets generated on the basis of viscous boundary layers. Detailed numerical simulations would also contribute to the understanding of the splashing phenomenon at high Weber numbers.

A sequence of events during splashing are showed in Figure 9 for $We = 3,500$ and $We = 10,000$. Three important events can be observed from this sequence. First, the amount of secondary droplets produced at $We = 3,500$ (see Figure 9(g)) is ap-

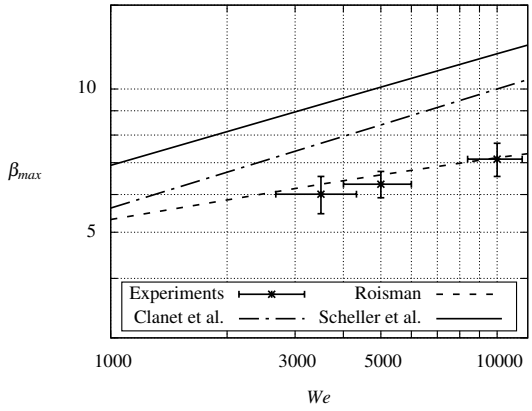

Fig. 8 Comparison of the maximal spreading diameter with models. The predicted maximal spreading diameter from Table 1 is plotted together with the mean and standard deviation (error bars) of all observations for each configuration, i.e., We=3,500; We=5,000, and We=10,000.

parently smaller than the amount produced at $We = 10,000$ (see Figure 9(g)). It seems that the higher the kinetic energy of the droplets, the greater the generated free surface, i.e. secondary droplets. Second, the secondary droplet generation is finished later at $We = 10,000$ than at $We = 3,500$. This can be clearly observed by comparing Figure 9(l) with Figure 9(x). Third, a crown is formed by the film only at $We = 3,500$ (Figures 9(d)-(f)), while at $We = 10,000$ it is not; instead, only secondary droplets are generated during the same period of time (Figures 9(p)-(r)). This observation was not expected, and more experiments are required to find out why no crown is formed at higher Weber numbers. Additionally, this outcome differs from the observations made by Faßmann, who reported that the number of secondary droplets should be smaller when the Weber number is increased.

The surrounding air played a significant role during the experiments. On the one hand, the rotation of the paddle generated a turbulent flow, which affected the trajectory of droplets. On the other hand, the pressure on the paddle increased with the angular velocity, showing that the droplets may reduce the velocity just before the impact. This was clearly observed when the Weber number was higher than 20,000. One possible explanation of the absence of crown formation at higher Weber number is that the high pressure on the surface suppresses it. Note that the presence of pressure correlates with the real situation when, for example, an airplane flies through a cloud and collides with water droplets. The droplets would impact first the aircraft nose, which has higher static pressure.

4 Conclusions

High-speed visualization was used to observe the impact of distilled water droplets with a glass surface at $We = 3,500$, $We = 5,000$, and $We = 10,000$. The images were recorded at 32,000 and 63,000fps from two different perspectives, which for the first time allowed to observe the evolution of splashing from the spreading diameter to the formation of secondary droplets at high Weber numbers.

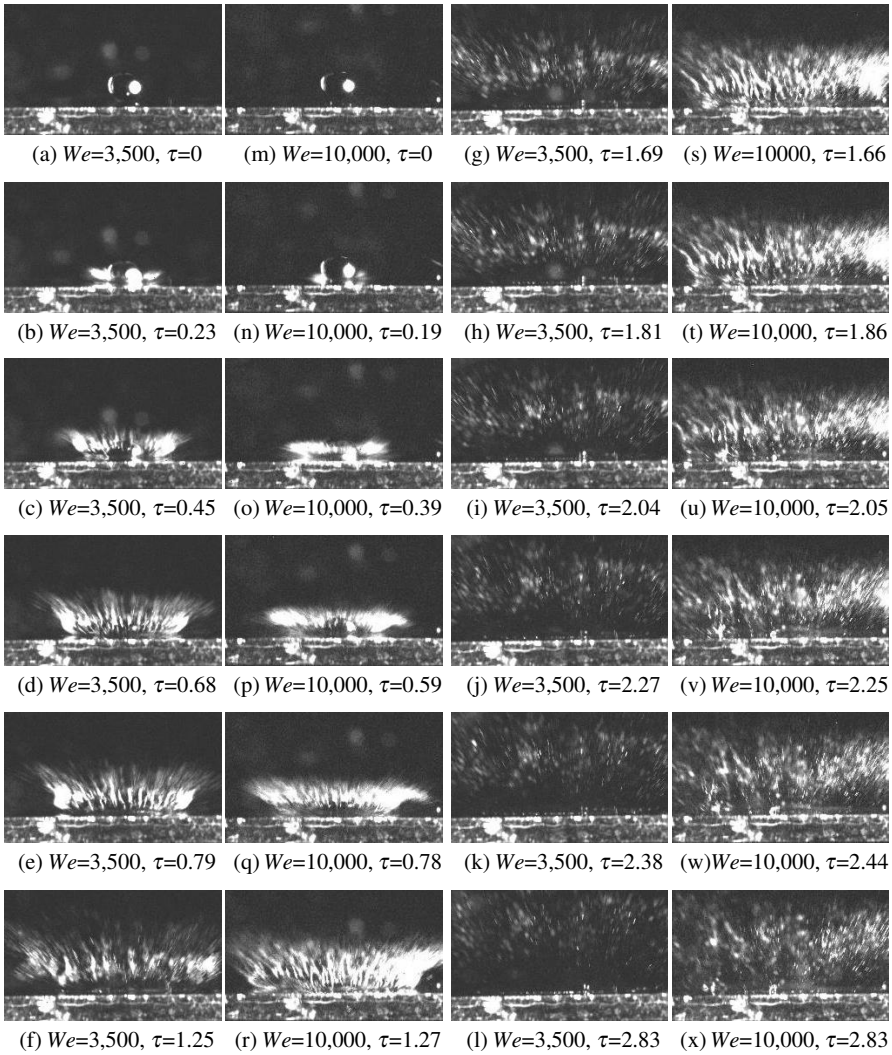

(a) We=3,500, τ=0 (m) We=10,000, τ=0 (g) We=3,500, τ=1.69 (s) We=10000, τ=1.66

(b) We=3,500, τ=0.23 (n) We=10,000, τ=0.19 (h) We=3,500, τ=1.81 (t) We=10,000, τ=1.86

(c) We=3,500, τ=0.45 (o) We=10,000, τ=0.39 (i) We=3,500, τ=2.04 (u) We=10,000, τ=2.05

(d) We=3,500, τ=0.68 (p) We=10,000, τ=0.59 (j) We=3,500, τ=2.27 (v) We=10,000, τ=2.25

(e) We=3,500, τ=0.79 (q) We=10,000, τ=0.78 (k) We=3,500, τ=2.38 (w)We=10,000, τ=2.44

(f) We=3,500, τ=1.25 (r) We=10,000, τ=1.27 (l) We=3,500, τ=2.83 (x) We=10,000, τ=2.83

Fig. 9: Time evolution of water droplets impacting with a glass plate at $We = 3,500$ (left) and $We = 10,000$ (right) over the dimensionless time τ. View from camera position 2, recorded at 32,000fps with $We = 3,500$ and 63,000fps with $We = 10,000$.

The experiments at high Weber numbers showed an unexpected similar behavior between the spreading diameters until the value of $\tau \approx 2$ was reached. It had a logarithmic character and was independent of the Weber or Reynolds numbers. The spreading rate $\dot{\beta}$ was described by a rational function, which only depends on time (see Eq. 2). Three different models of the maximal spreading diameter were analyzed and compared with the experiments. The tendency of some models was

to overestimate the maximal spreading diameter by more than 40%. However, the model presented by Roisman [9] accurately predicted β_{max} for high Weber numbers. This demonstrates that a theory involving the viscous boundary layers is more appropriate for the description of β. The observations also showed that the higher the Weber number, the greater the mass of secondary droplets. No crown was observed at $We = 5,000$ and $We = 10,000$; instead, only secondary droplets were ejected at the early stage of splashing. This prompt splash was not expected using a smooth glass surface, and, contrary to the spreading rate, it seems to depend on the Weber and Reynolds numbers.

This work has contributed to the validation of the most common models of the spreading diameter. Additionally, it has provided information about the time development of the mass that has stuck on the surface and the secondary droplets during splashing. Further experimental and numerical studies are planned in the near future in order to establish the relationship between the mass of the stuck droplet and the secondary droplets at high Weber number. The forces during splashing would need to be investigated in the future using the new data obtained at even higher Weber numbers.

Acknowledgements We are thankful to the deutsche Forschungsgemeinschaft (DFG) for the financial support and to Cameron Tropea from the Technische Universität Darmstadt for the loan of the high-speed camera.

References

1. Bansmer S, Steiner J (2016) Ice Roughness and Its Impact on the Ice Accretion Process. 8th AIAA Atmospheric and Space Enviroments Conf., AIAA 2016-3591
2. Clanet C, Bguin C, Richard D, Quere D (2004) Maximal deformation of an impacting drop. J Fluid Mech 517:199-208
3. Faßmann B, Bansmer S, Möller T, Radespiel R (2013) High velocity impingement of single droplets on a dry smooth surface. Exp Fluids 54:1516
4. Faßmann B (2015) Zeitabhängige Charakterisierung der Sekundärtropfen aus dem Hochgeschwindigkeitsaufprall einzelner Flüssigkeitstropfen. Dissertation. Technische Universität Braunschweig
5. Josserand C, Thoroddsen S (2016) Drop Impact on a Solid Surface. Annu Rev Fluid Mech 48:365-91
6. Mehdizadeh N, Chandra S, Mostaghimi J (2000) Splashing of a small droplet impinging on a solid surface at high velocity. In: Kim JH (ed) Proceedings of the ASME heat transfer division 2000, vol 3. American Society of Mechanical Engineers, New York and NY, HTD, pp 397-405.
7. Mehdizadeh N, Chandra S, Mostaghimi J (2004) Formation of fingers around the edges of a drop hitting a metal plate with high velocity. J Fluid Mech 510:353-373
8. Rioboo R, Mareng M, Tropea C (2002) Time evolution of liquid impact onto solid, dry surfaces. Exp Fluids 33:112-124
9. Roisman I (2009) Inertia dominated drop collisions. II. An analytical solution of the Navier-Stokes equations for spreading viscous film. Physics of Fluids 21, doi:10.1063/1.3129283
10. Scheller B, Bousfield D (1995) Newtonian Drop Impact with a Solid Surface. AIChE J 41:1357-67
11. Thoroddsen S (2002) The ejecta sheet generated by the impact of a drop. J Fluid Mech 451:373-381
12. Zhang C, Liu H (2016) Effect of drop size on the impact thermodynamics for supercooled large droplet in aircraft icing. Physics of Fluid 28, doi:10.1063/1.4953411